Inverse Patchy Colloids: From Microscopic Description to Mesoscopic Coarse-Graining

Emanuela Bianchi[*a,b], **Gerhard Kahl**[a] **and Christos N. Likos**[c,b]

Typically, patchy systems are characterized by the formation of a small number of directional, possibly selective, bonds due to the presence of attractive regions on the surface of otherwise repulsive particles. Here, we consider a new type of particles with patterned surfaces and we refer to them as *inverse patchy colloids* because, in this case, the patches on the repulsive particles repel each other instead of attracting. Further, these patches attract the parts of the colloid that are free of patches. Specifically, we consider heterogeneously charged colloids consisting of negatively charged spherical particles carrying a small number of positively charged patches. Making use of the Debye-Hückel theory, we derive the effective interaction potential between a pair of inverse patchy colloids with two patches on opposite poles. We then design a simple coarse-grained model via a mapping with the analytical pair potential. The coarse-grained model quantitatively reproduces the features of its microscopic counterpart, while at the same time being characterized by a much higher degree of computational simplicity. Moreover, the mesoscopic model is generalizable to an arbitrary number of patches.

1 Introduction

In recent years, patchy particles, i.e., colloids with inhomogeneously patterned surfaces, have attracted tremendous interest of both experimentalists and theoreticians (for a recent overview in experiments and theory see Ref.[1] and Ref.[2], respectively). Typical examples of patchy particles are spherically symmetric, mutually repulsive colloids decorated on their surface by a small number of extended, attractive regions. The effective interaction between these particles is characterized by a well-defined anisotropy, making patchy particles ideal candidates as building entities, bringing about complex self-assembly scenarios in soft matter physics. Nowadays, experimental techniques both in the nano- and micro-scale allow to position the patches on well-defined arrangements and, possibly, to control their spatial extent on the colloidal surface, see e.g. Ref.[3–8]. On the other hand, theoreticians have succeeded to develop in parallel suitable models that mimic these highly directional interactions[2]. Using theoretical methods and computer simulations, structural and thermodynamic properties as well as the self-assembly scenarios of these model systems have been, and still are, widely investigated.

In the present paper, we introduce a novel class of patchy particles, which we term *inverse patchy col-*

[0*] *E-mail: bianchi@cmt.tuwien.ac.at; Tel: +43 1 5880113631; Fax: +43 1 5880113699*

[0a] *Institut für Theoretische Physik, Technische Universität Wien, Wiedner Hauptstrasse 8-10, A-1040 Vienna, Austria.*

[0b] *Institut für Theoretische Physik, Heinrich-Heine-Universität Düsseldorf, Universitätstraße 1, D-40225 Düsseldorf, Germany.*

[0c] *Faculty of Physics, University of Vienna, Boltzmanngasse 5, A-1090 Vienna, Austria.*

loids (IPCs), referring to the repulsive nature of the patches as opposed to common attractive patches. Our motivation resides in a recently presented colloidal system[9] made of negatively charged, spherical colloids onto which positively charged polyelectrolyte stars are adsorbed. When the charge ratio between polyelectrolytes and colloids is such that only two stars adsorb onto the colloidal surface, the polyelectrolytes stars occupy the two polar regions of the colloid, while the equatorial region remains uncovered. The resulting complex is an heterogeneously charged particle with positive polar patches and a negative equatorial region. Due to the repulsion between charge-like surfaces, the effective interaction between two IPCs can be both attractive and repulsive, according to the relative orientation of the two particles: polar, as well as equatorial, regions are mutually repulsive, while polar and equatorial regions attract each other. In contrast to conventional patchy particles, attraction and repulsion in inverse patchy systems play a role on an equal footing, allowing for even more widespread self-assembly scenarios than patchy particles. We note that, under suitable conditions of charge- and size-asymmetries, also more than two polyelectrolyte stars can be adsorbed on the colloidal sphere. The presentation in the manuscript is restricted to the two patches case, but we also discuss the generalization to an arbitrary number of patches at the end.

In this contribution, we wish to propose a general model for colloids with two positive polar patches on their negatively charged surface, pointing out a way to coarse-grain a class of systems referred to as inverse patchy colloids. We develop a theoretical description for the effective interaction potential between two IPCs carrying two patches. Based on the Debye-Hückel (DH) theory, we derive the fully analytic expression for the total electrostatic potential, $\Phi(\mathbf{r})$, around one single IPC. The resulting expression, involving both Legendre polynomials and modified spherical Bessel functions of the third kind, can be complex to be used in the derivation of the effective pair interaction between two IPCs. Nonetheless, under high screening conditions, $\Phi(\mathbf{r})$ can be factorized in a radially symmetric Yukawa contribution, which depends only on $r = |\mathbf{r}|$, and an angle dependent factor that takes into account the non-spherically symmetric charge distribution. Such a simplification allows us to analytically derive the effective pair potential between two IPCs.

In an effort to make our model of IPCs amenable to investigations of collective behaviors of many body systems, we develop a coarse-grained (CG) picture of the effective interactions between two IPCs. This simplified model is accessible directly from the colloidal model system (cf. schematic representation in Fig. 1), but it shows a straightforward relation with the DH description. Indeed, the three charges of the microscopic DH model are replaced, in a way that fully preserves the original arrangements of the patches, by three interaction spheres: a big sphere around the impenetrable particle and two small, out-of-center spheres; the latter ones represent the patches and are immersed to a large extent in the particle. We assume for all three interaction ranges the same value δ, the latter being set by the microscopically-determined screening length of the electrostatic interactions, common to both repulsions and attractions. The effective interaction between two coarse-grained IPCs can now be simply written as the sum over three contributions, which stem from the different overlap scenarios of the two types of interaction spheres. Further, each of these contributions is postulated to factorize in an energetic and a purely orientational-geometric contribution; the latter one can be suitably tabulated and is thus amenable to numerical investigations.

The relation of our coarse-grained model to the IPC model system can take advantage of the available analytical description at the microscopic level, strengthening thereby the link between the underlying physical system and its coarse-grained counterpart. The parameters of the coarse-grained model are chosen via a direct mapping to the DH model (cf. schematic representation in Fig. 1): the interaction sphere distribution of the mesoscopic model is assumed to have the same eccentricity of the discrete charge distribution within the DH description, while the interaction range for a pair of coarse-grained IPCs is related to the Debye

screening length. Further, we propose two different procedures to establish the above mentioned energetic prefactors in the coarse-grained pair interaction energy. We then discuss in detail the results that we obtain for the effective potentials via the different routes.

The paper is organized as follows: in Sections 2 and 3 the DH and the coarse-grained model are presented, respectively. In Section 4 we propose a mapping scheme to relate these two models and results for the ensuing effective potentials are discussed in Section 5. The main text of the manuscript is closed with concluding remarks. The paper is supplemented by two appendices: Appendix A deals with the linearization scheme of the DH approach, while in Appendix B we present the details on how the exact expression for the electrostatic potential generated by one IPC within the DH picture can be simplified under high screening conditions.

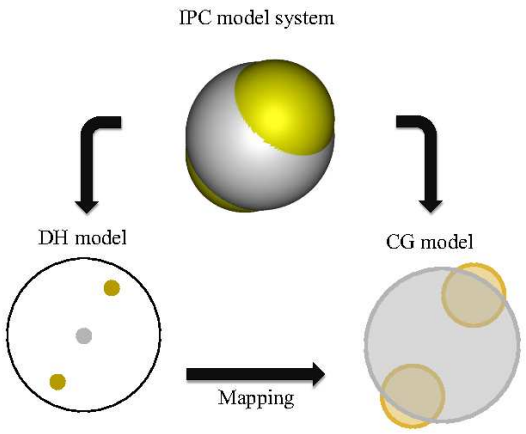

Figure 1: (Color online). Top: three-dimensional representation of an inverse patchy colloid (IPC) with two polar patches. The (yellow) polar patches and the (grey) equatorial region have positive and negative surface charge, respectively. Bottom: the microscopic Debye-Hückel (DH) description (left side) and the mesoscopic coarse-grained (CG) model (right side). In the DH-model, the (grey) central sphere is the center of charge of the colloid and the two (yellow) out-of-center spheres are the centers of charge of the attached patches. The coarse-grained model reproduces the symmetries of the heterogeneous charge distribution of the IPC model system. The parameters of such a simple model are chosen by taking advantage of the underlying DH analytical description.

2 Debye-Hückel microscopic description of IPCs

The statistical mechanical approach to electrolytes treats the electrolytic solution as a suspension of impenetrable, charged colloidal particles in a liquid dielectric solvent containing co- and counter-ions. For a linear, homogeneous and isotropic dielectric medium, the Maxwell equations of electrostatics lead (in the absence of external fields) to a differential equation of Poisson type, which relates the electrostatic potential of the system with the ionic charge density distribution[10]. In a mean field approach, the equilibrium charge

density obeys Boltzmann statistics; the resulting equation that describes the electrostatic potential, known in literature as the Poisson-Boltzmann equation, is an intrinsically non-linear differential equation[11]. The linearized Poisson-Boltzmann approach is referred to as the DH description[12]. Although stricktly suitable only for the dilute case, it provides surprisingly good results also for denser systems[13]. The extentions to concentrated solutions often require the replacement of the bare colloidal charge Z with a so-called effective[14] DH-charge Z^*, which takes into account the strong condensation of counter-ions on the Stern-layer around the colloids. Further, it is possible to employ a rescaling of the inverse Debye screening length κ to take into account free volume effects[15] or to adjust κ with the goal of describing experimental results[16]. At any rate, the functional form of the DH-potential can be preserved and it provides for a realistic description of experimental data for a vast variety of physical situations.

According to Gauss law, the electrostatic field surrounding a spherical colloid with a homogeneously distributed surface charge is identical to the field generated by a point charge positioned in the center of the dielectric colloidal particle. By replacing the surface charge with a point charge located in the center of the colloid, the DH approach leads to the traditional Derjaguin-Landau-Verwey-Overbeek (DLVO) pair interaction[17].

In this paper we deal with *heterogeneously charged* particles: we consider negatively charged colloids decorated by a small number of positively charged surface regions (so-called patches). Following the ideas presented in Ref.[18], we replace the heterogeneous surface charge with a non-spherically symmetric distribution of discrete charges inside the colloidal particle: the charge of the colloidal surface and of the patches are replaced by point charges positioned at their respective centers of charge. Within the DH approach, we derive an analytical expression of the screened electrostatic potential generated by a single IPC (Sec. 2.1). Based on this information, we construct the effective interaction potential between a pair of IPCs (Sec. 2.2).

2.1 The electrostatic potential around one IPC

We consider a spherical, heterogeneously charged colloid of radius σ with a negatively charged equatorial region and two positively charged polar regions, the patches. According to the scheme outlined above, the total surface charge of the colloid ($Z_c q_e < 0$) and the charges of the two patches ($Z_p q_e > 0$, each), q_e being the positive elementary charge, are replaced by equivalent point charges positioned at the corresponding centers of charge inside the colloidal sphere. While the colloidal center of charge coincides – due to the spherical symmetry – with the center of the colloidal sphere, the centers of charge of the two patches are located at a distance $a(\leq \sigma)$ from the center, diametrically opposite to each other; a is termed the asymmetry of the discrete charge distribution (see Fig. 2). From the inner part of the sphere, denoted as region I, both co- and counter-ions are excluded, while region II is the medium containing the ions of the electrolytic solution. For sake of simplicity we assume the dielectric permittivity to have the same value in both regions, namely ε. We note that the more general case has been treated in Ref[18]. Due to the cylindrical symmetry of the charge distribution, we can assume that the three centers of charge lie on the z axis. We introduce spherical coordinates (r, θ, ϕ) with the origin in the center of the colloidal particle. Due to the azimuthal symmetry of the charge distribution, the resulting electrostatic potential depends only on r and θ (see Fig. 2), and thus the solutions of the electrostatic problem can be expanded in Legendre Polynomyals $P_l(\cos\theta)$. For the more general case, the latter should be replaced by the spherical harmonics $Y_{lm}(\theta, \phi)$, see Ref.[18] for details.

We now derive the total screened electrostatic potential, $\Phi(r, \theta)$, that an IPC generates in space. Let

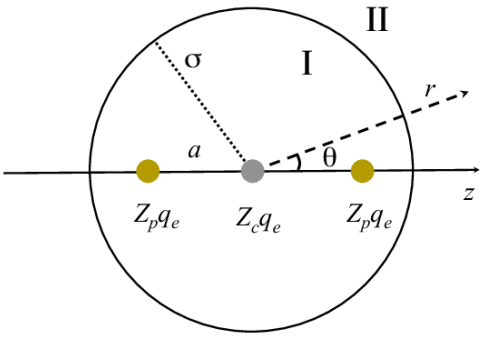

Figure 2: (Color online). Two dimensional representation of the DH scheme for an inverse patchy colloid with two positively charged poles and a negatively charged equatorial region. The spherical colloid, denoted as region I, is surrounded by the solvent, denoted as region II. The dielectric permittivity is chosen to be the same in both regions and it is denoted by ε in the text. The colloidal sphere of radius σ contains in its inside three point centers of charge represented by dots (grey for the negative charge and yellow for the positive ones) along the z axis inside the colloidal sphere. The point-like co- and counter-ions in region II are not shown. The negative charge in the center of the colloidal sphere has value $Z_c q_e$, where q_e is the magnitude of the elementary charge and $Z_c < 0$. The two positive charges have value $Z_p q_e$ each and lie at a distance a from the colloidal center, one opposite to the other.

$\Phi^{\rm I}(r,\theta)$ and $\Phi^{\rm II}(r,\theta)$ be the expressions for $\Phi(r,\theta)$ in the interior and the exterior of the colloidal particle, respectively. For $r < \sigma$, $\Phi(r,\theta)$ is determined via the Poisson equation for the discrete distribution of three charges, while for $r > \sigma$ we assume that the linearized Poisson-Boltzmann equation holds (see Appendix A); these equations read as

$$\begin{aligned} \nabla^2\Phi^{\rm I}(r,\theta) &= -\frac{4\pi}{\varepsilon} Z_p q_e \left[\delta(\vec{r}-a\hat{z}) + \delta(\vec{r}+a\hat{z})\right] - \frac{4\pi}{\varepsilon} Z_c q_e \delta(\vec{r}) \qquad r < \sigma \\ \nabla^2\Phi^{\rm II}(r,\theta) &= \kappa^2 \Phi^{\rm II}(r,\theta) \qquad r > \sigma. \end{aligned} \tag{1}$$

Here κ^{-1} is the Debye screening length which is determined by the bulk number densities ρ_i^0 of the mobile, ionic species (with valences Z_i) in the solution: $\kappa^2 = \frac{4\pi q_e^2}{\varepsilon k_B T} \sum_i \rho_i^0 Z_i^2$, where T is the temperature and k_B is the Boltzmann constant.

To solve the system of differential equations (1), we need to consider the proper boundary conditions: (i) $\Phi(r,\theta)$ must vanish at infinity and be continuous in $r = \sigma$, and (ii) at the interface between regions I and II, the tangential component of the electrostatic field and (in the absence of surface charges) the normal component of the displacement field must be continuous [18].

We are interested only in the screened electrostatic potential outside the colloid. Thus, omitting in the

following the superscript II, the electrostatic potential in the region of interest is

$$\begin{aligned}\Phi(r,\theta) &= \frac{(Z_c+2Z_p)q_e}{\varepsilon}\frac{\exp(\kappa\sigma)}{1+\kappa\sigma}\frac{\exp(-\kappa r)}{r} \\ &+ \frac{2Z_p q_e}{\varepsilon}\sum_{l=2}^{\infty}{}'\left(\frac{a}{\sigma}\right)^l\frac{(2l+1)}{\kappa\sigma\sqrt{r\sigma}}\frac{K_{l+1/2}(\kappa r)}{K_{l+3/2}(\kappa\sigma)}P_l(\cos\theta),\end{aligned} \tag{2}$$

where the prime indicates that the sum runs over even index values l only, $P_l(\cos\theta)$ are the Legendre polynomials of order l, $K_{l+1/2}(z)$ and $K_{l+3/2}(z)$ are modified spherical Bessel functions of the third kind[19]. In Appendix A, we use the analytical expression of $\Phi(r,\theta)$ to confirm the reliability of the DH approximation in the parameter space.

As explicitly derived in Appendix B, when $\kappa\sigma \gtrsim 1$ the ratio between spherical Bessel functions of consecutive orders is proportional to $\exp(-\kappa r)/r$. Hence, under high screening conditions, it is possible reduce Eq. (2) for the total electrostatic potential of an IPC to a simpler, Yukawa-like expression, where the angular and the radial contributions factorize, i.e.

$$\Phi(r,\theta) = \bar{\Phi}(\theta)\frac{\exp(-\kappa r)}{r}, \tag{3}$$

with

$$\bar{\Phi}(\theta) = \frac{\exp(\kappa\sigma)}{\varepsilon(1+\kappa\sigma)}\left[Z_c q_e + 2Z_p q_e\sum_{l=0}^{\infty}{}'\left(\frac{a}{\sigma}\right)^l(2l+1)P_l(cos\theta)\right]. \tag{4}$$

The effect of the approximation on $\Phi(r,\theta)$ is discussed in Appendix B. We show that, in the considered parameter space, the approximate expression for the electrostatic potential yields numerical values of the same order of magnitude as the analytic expression, even at the colloidal surface (see Fig. 10).

2.2 The pair interaction between two IPCs

We now consider two identical IPCs, labeled with indices i and j, and, starting from the total electrostatic potential generated by each of them [see Eqs. (3) and (4)], we derive their effective interaction. Let $\vec{r}_{ij}$ be the vector connecting the centers of two IPCs, let $\hat{n}_i$ and $\hat{n}_j$ be the unit vectors that specify the orientations of colloids i and j, respectively, and let us define the angles between the orientational unit vectors of the colloids and their center-to-center unit vector as $\theta_i = \cos^{-1}(\hat{n}_i\cdot\hat{r}_{ij})$ and $\theta_j = \cos^{-1}(\hat{n}_j\cdot\hat{r}_{ij})$. Furthermore, let us define the angle between the orientational unit vectors of the two IPCs as $\theta_{ij} = \cos^{-1}(\hat{n}_i\cdot\hat{n}_j)$.

The effective pair interaction potential, $\psi(r_{ij},\theta_i,\theta_j,\theta_{ij})$, that we will derive in the following, has to be symmetric with respect to the indices i and j. Hence, we consider the potential energy, ψ_{ij}, due to the presence of colloid j in the screened electrostatic field generated by colloid i and its surrounding ions; ψ_{ji} is similarly derived for the inverse situation. Then, we make the symmetrization *ansatz*: $\psi = (\psi_{ij}+\psi_{ji})/2$, ommitting for the moment the arguments. We outline in the following the derivation for ψ_{ij}. The potential energy ψ_{ij} is given by the sum over all the contributions from the three charges inside colloid j. In analogy to the derivation of the DLVO potential, we take into account the fact that microscopic co- and counter-ions

cannot penetrate the IPC by replacing the bare charges with effective charges:

$$\tilde{Z}_j^m = \begin{cases} Z_c q_e \frac{\exp(\kappa\sigma)}{1+\kappa\sigma} & \text{if } m = 0 \\ \\ Z_p q_e \frac{\exp(\kappa\sigma)}{1+\kappa\sigma} & \text{if } m = 1,2, \end{cases} \tag{5}$$

where we have used $m = 0$ for the central charge and $m = 1,2$ for the out-of-center charges. Hence, ψ_{ij} is given by[10,20]

$$\psi_{ij}(r_{ij},\theta_i,\theta_j,\theta_{ij}) = \psi_{ij}(r_{ij},\theta_i,\theta_i^1,\theta_i^2) = \sum_{m=0,1,2} \tilde{Z}_j^m \Phi(r_{ij}^m,\theta_i^m). \tag{6}$$

Here, the r_{ij}^m are the lengths of the vectors joining the centre of colloid i with the three centers of charges inside colloid j, and the θ_{ij}^m are the corresponding angles, as shown in Fig. 3. Note that $r_{ij}^0 \equiv r_{ij}$ and $\theta_{ij}^0 \equiv \theta_{ij}$. By applying the law of cosines on the triangles defined by $\vec{r}_{ij}^{1,2}$, $\hat{n}_j$ and $\vec{r}_{ij}$, we have $r_{ij}^{1,2} = (a^2 + \vec{r}_{ij}\cdot\vec{r}_{ij} \mp 2ar_{ij}\cos\theta_j)^{1/2}$. In Eq. (6), the explicit dependence of ψ_{ij} has been expressed taking into account that θ_i^1 and θ_i^2 are determined once θ_j and θ_{ij} are fixed, and vice versa.

By defining the dimensionless quantities $\xi_{1,2} = r_{ij}^{1,2}/r_{ij}$, we can now explicitly write down $\psi_{ij}(r_{ij},\theta_i,\theta_i^1,\theta_i^2)$ in a DLVO-like expression, i.e.

$$\psi_{ij} = \frac{Q_{ij}(r_{ij},\theta_i,\theta_i^1,\theta_i^2) q_e^2}{\varepsilon} \left(\frac{\exp(\kappa\sigma)}{1+\kappa\sigma}\right)^2 \frac{\exp(-\kappa r_{ij})}{r_{ij}}, \tag{7}$$

where $Q(r_{ij},\theta_i,\theta_i^1,\theta_i^2)$ is an orientationally dependent factor, which takes into account all the charge valences involved in the interaction:

$$\begin{aligned} Q_{ij}(r_{ij},\theta_i,\theta_i^1,\theta_i^2) &= \left[Z_c^2 + 2Z_c Z_p \sum_{l=0}^{\infty}{}' (2l+1) \left(\frac{a}{\sigma}\right)^l P_l(\cos\theta_i) \right] \\ &+ \left[Z_c Z_p + 2Z_p^2 \sum_{l=0}^{\infty}{}' (2l+1) \left(\frac{a}{\sigma}\right)^l P_l(\cos\theta_i^1) \right] \frac{\exp\left[-\kappa r_{ij}(\xi_1 - 1)\right]}{\xi_1} \\ &+ \left[Z_c Z_p + 2Z_p^2 \sum_{l=0}^{\infty}{}' (2l+1) \left(\frac{a}{\sigma}\right)^l P_l(\cos\theta_i^2) \right] \frac{\exp\left[-\kappa r_{ij}(\xi_2 - 1)\right]}{\xi_2}. \end{aligned} \tag{8}$$

By following an analogous procedure, we obtain an expression for ψ_{ji}, leading finally to the total symmetric pair potential between two IPCs $\psi(r_{ij},\theta_i,\theta_j,\theta_{ij})$. In the following we refer to $\psi(r_{ij},\theta_i,\theta_j,\theta_{ij})$ as the DH pair potential between two IPCs.

It is worth noting that for ψ_{ij} given in Eqs. (7) and (8) the DLVO limits can easily be recovered. Trivially, if $Z_p \to 0$, then $Q_{ij} \to Z_c^2$ and Eq. (7) reduces to the DLVO interaction between two colloids, each of them carrying a homogeneously distributed charge $Z_c q_e$. Furthermore, if $Z_p \neq 0$ and $a \to 0$, Eq. (7) reduces again to a DLVO-like potential. Indeed, in the latter limit, only the $l = 0$ terms survive in Eq. (8), while $\xi_{1,2} \to 1$, so that the exponential factors in Q_{ij} goes to unity. The final expression for the pair potential is then

$$\psi(r_{ij}) = \frac{(Z_c^2 + 4Z_c Z_p + 2Z_p^2) q_e^2}{\varepsilon} \left(\frac{\exp(\kappa\sigma)}{1+\kappa\sigma}\right)^2 \frac{\exp(-\kappa r_{ij})}{r_{ij}}, \tag{9}$$

which is the DLVO potential of a pair of colloids, each of them carrying a total charge $(Z_c + 2Z_p)q_e$.

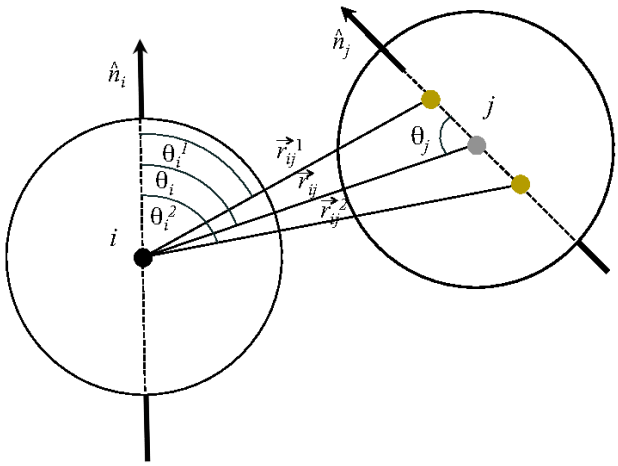

Figure 3: (Color online). Schematic representation of a pair of IPCs at a fixed distance r_{ij}. To calculate ψ_{ij}, we consider j as a spherical particle carrying three discrete point charges as in Fig. 2, while we consider i as the point source of the screened electrostatic field. Here, $\hat{n}_i$ and $\hat{n}_j$ are the orientational unit vectors of particle i and j, θ_i and θ_j are the corresponding angles between such orientational vectors and the center-to-center vector between the two IPCs, $r_{ij}^{1,2}$ are the vectors joining the center of i with the two out-of-center points in j, and $\theta_{ij}^{1,2}$ are the corresponding angles between such vectors and $\hat{n}_i$. Please note that $\hat{n}_i$ and $\hat{n}_j$ are not generally in the same plane: the angle between them is defined by θ_{ij} (not shown in the figure). As a consequence, neither $\vec{r}_{ij}$, $\vec{r}_{ij}^{1}$ and $\vec{r}_{ij}^{2}$ are in the same plane.

3 The coarse-grained mescoscopic model of IPCs

As described in the Introduction, we deal with heterogeneously charged colloids having a negatively charged equatorial region and two positively charged polar regions. The microscopic analytical description of the model system is provided by applying the DH theory of dilute electrolytes. Nonetheless, the analytic potential derived in Sec. 2 may be cumbersome for numerical simulation techniques. In order to study the collective behaviors of inverse patchy colloidal systems, a coarse graining procedure is of great importance. We propose a coarse-grained model of our IPCs with the goal of dealing with a more feasible pair potential description, while keeping a close connection to the physical system. In particular, the coarse-grained model is constrained to respect the following conditions, making it strongly linked to the original DH-model:

(i) It preserves in full the geometrical arrangement of the patches.

(ii) As a consequence, it has exactly the same symmetries as the original system.

(iii) It maintains the “mixed”, attractive/repulsive character of the former, depending on interparticle orientations.

(iv) The energy and length scales involved in the coarse-grained model are derived from their microscopic counterparts and are closely related to them.

At the same time, we achieve dramatic computational simplification by further introducing a factorization of the coarse-grained model into energetic and geometrical contributions (see below).

The basic feature of a IPC is a three-regions surface: an equator and two poles having different mutual and crossed properties. When designing such a patterned surface, we take into account that delocalized, soft patches better suit the nature of the electrostatic interactions. Moreover, we prefer to have a flexible patchy model with three independent sets of parameters: the interaction ranges, the interaction strengths, and the patch surface coverage. Inspired by the Kern-Frenkel model[21], we design a simple inverse patchy colloid as described in the following.

3.1 Design of the patchy model

In an effort to design a simple model for IPCs, we consider a spherical, impenetrable colloidal particle of radius σ. The hard-core models steric constraints and guarantees the thermodynamic stability of the system. The corresponding interaction sphere has radius $\sigma+\delta/2$, where δ is the interaction range specified below. Inside the hard colloid, two interaction sites are located at a distance $e(\leq\sigma)$ in opposite directions from the particle center (see Fig. 4); e is termed the *eccentricity* of the model. The interaction sphere of each of these sites is an out-of-center sphere of radius ρ, submerged in the colloid to an extent that is fixed by e. The geometrical arrangement of the interaction spheres defines three regions on the surface of the hard core particle. In the following, we refer to the two types of interaction spheres as big spheres of radius $R_B=\sigma+\delta/2$ (labeled B) and small spheres of radius $R_S=\rho$ (labeled S). In such a description, the potentials between the big spheres and the small spheres are repulsive, representing the interaction between equatorial regions and patches, respectively; in contrast, the potential between big and small spheres is attractive, representing the interaction between the equatorial regions and patches.

Since in the microscopic system the interaction range of two IPCs is determined by the electrostatic screening, we assume the BB, the BS and the SS interactions to have the same range δ. Such an assumption implies the following relation between the parameters (see Fig 4):

$$\delta = 2(e+\rho)-2\sigma, \tag{10}$$

i.e., the small spheres are tangential to the big sphere, as shown in Fig. 4. Of course $e+\rho\geq\sigma$, since $\delta>0$. Furthermore, we define the opening angles γ and $(\pi-2\gamma)$, characterizing the extension of the polar and the equatorial regions, respectively. The following restriction holds:

$$\cos\gamma = \frac{\sigma^2+e^2-\rho^2}{2\sigma e}. \tag{11}$$

Since the extension of one single patch is limited to a hemisphere, e and ρ can only be varied in such a way as to guarantee $\gamma<\pi/2$. We note that, for a given value of δ, the choice of the ratio ρ/e defines γ, i.e., we can take into account different patch extensions, while keeping fixed the interaction range. Once e and ρ, being the two independent parameters of the model, are defined, the physical parameters, i.e., the interaction range δ and the patch extension γ, are given by Eq. (10) and (11), respectively.

Defining the distance between two IPCs and their orientational unit vectors as in Sec. 2.2, the coarse-grained pair interaction potential between two IPCs within our model is

$$V(r_{ij},\theta_i,\theta_j,\theta_{ij}) = \begin{cases} \infty & \text{if } r_{ij}<2\sigma \\ U(r_{ij},\theta_i,\theta_j,\theta_{ij}) & \text{if } 2\sigma\leq r_{ij}\leq 2\sigma+\delta. \\ 0 & \text{if } 2\sigma+\delta<r_{ij} \end{cases} \tag{12}$$

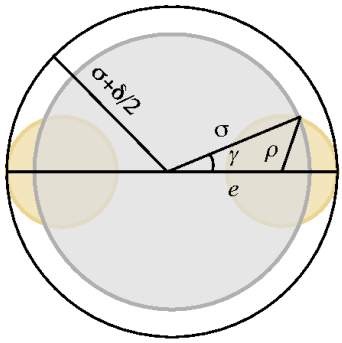

Figure 4: (Color online). Two dimensional picture of the coarse-grained model of a IPC. The colloid's impenetrable volume is represented by the (grey) circle of radius σ, the big (black) circle of radius $\sigma+\delta/2$ represents the interaction volume of the colloid, while the two small (yellow) circles of radius ρ represent the interaction volumes of the two sites, positioned at distance e from the colloidal center, one opposite to the other, on an in-line geometry. The interaction range, δ, and the surface extension, γ, of the patches are related to the model parameters e, ρ and σ by Eq. (10) and (11), respectively.

The function $U(r_{ij},\theta_i,\theta_j,\theta_{ij})$ is the sum over three contributions stemming from the BB, the BS and the SS interactions. We postulate that each of these contributions can be factorized into an energy strength and a geometrical weight factor. The former ones are suitable defined (see Sec. 4) energy contributions $u_{\alpha\beta}$, while the latter ones are dimensionless weight factors $w_{\alpha\beta}$, which take into account the dependence of the pair potential on both the distance r_{ij} and the relative orientation of the two IPCs via the three angles (with αβ = BB, SS, or BS). Hence we have

$$U(r_{ij},\theta_i,\theta_j,\theta_{ij}) = w_{\mathrm{BB}}u_{\mathrm{BB}} + w_{\mathrm{BS}}u_{\mathrm{BS}} + w_{\mathrm{SS}}u_{\mathrm{SS}}. \tag{13}$$

In order to simplify the notation, we have suppressed in the above equation the explicit dependence of the $w_{\alpha\beta}$ on r_{ij}, θ_i, θ_j and θ_{ij}. We choose each weight factor to be proportional to the total overlap volume, $\Omega_{\mathrm{O_T}}^{\alpha\beta}$, of all interaction spheres contributing to the specific αβ interaction, i.e.,

$$w_{\alpha\beta} = \Omega_{\mathrm{O_T}}^{\alpha\beta}/\Omega_{\mathrm{R}}. \tag{14}$$

Here Ω_{R} is a normalizing reference volume, which is chosen to be volume of the colloidal hard sphere, i.e., $\Omega_{\mathrm{R}} = \frac{4}{3}\pi\sigma^3$. The $\Omega_{\mathrm{O_T}}^{\alpha\beta}$ for the three possible interaction types are given by

$$\Omega_{\mathrm{O_T}}^{\mathrm{BB}} = \Omega_{\mathrm{O}}^{\mathrm{B}_i\mathrm{B}_j} \tag{15}$$

$$\Omega_{\mathrm{O_T}}^{\mathrm{BS}} = \Omega_{\mathrm{O}}^{\mathrm{B}_i\mathrm{S}_j^1} + \Omega_{\mathrm{O}}^{\mathrm{B}_i\mathrm{S}_j^2} + \Omega_{\mathrm{O}}^{\mathrm{B}_j\mathrm{S}_i^1} + \Omega_{\mathrm{O}}^{\mathrm{B}_j\mathrm{S}_i^2} \tag{16}$$

$$\Omega_{\mathrm{O_T}}^{\mathrm{SS}} = \Omega_{\mathrm{O}}^{\mathrm{S}_i^1\mathrm{S}_j^1} + \Omega_{\mathrm{O}}^{\mathrm{S}_i^1\mathrm{S}_j^2} + \Omega_{\mathrm{O}}^{\mathrm{S}_i^2\mathrm{S}_j^1} + \Omega_{\mathrm{O}}^{\mathrm{S}_i^2\mathrm{S}_j^2}, \tag{17}$$

where i and j ($i \neq j$) denote the indices of two interacting IPCs. Again, the dependence on distances and orientational angles has not been explicitly expressed.

Let us now consider two different spheres of radii R_α and R_β, respectively, and separated by a distance $r_{\alpha\beta}$, where α and β = B or S. Then, the overlap volume between these two spheres is given by

$$\Omega_{\rm O}^{\alpha\beta}(r_{\alpha\beta}) = \begin{cases} 0 & \text{if } r_{\max} \leq r_{\alpha\beta} \\ \frac{\pi}{3}\left[\left(2R_\alpha + \frac{R_\alpha^2 - R_\beta^2 + r_{\alpha\beta}^2}{2r_{\alpha\beta}}\right)\left(R_\alpha - \frac{R_\alpha^2 - R_\beta^2 + r_{\alpha\beta}^2}{2r_{\alpha\beta}}\right)^2\right] + & \\ \frac{\pi}{3}\left[\left(2R_\beta - \frac{R_\alpha^2 - R_\beta^2 - r_{\alpha\beta}^2}{2r_{\alpha\beta}}\right)\left(R_\beta + \frac{R_\alpha^2 - R_\beta^2 - r_{\alpha\beta}^2}{2r_{\alpha\beta}}\right)^2\right] & \text{if } r_{\min} \leq r_{\alpha\beta} \leq r_{\max} \\ \frac{4}{3}\pi R_<^3 & \text{if } r_{\alpha\beta} \leq r_{\min}. \end{cases} \tag{18}$$

Here, $R_<$ =min(R_α, R_β), $r_{\max} \equiv R_\alpha + R_\beta$ is the distance above which the two spheres do not overlap anymore, and $r_{\min} \equiv |R_\alpha - R_\beta|$ is the distance below which the two spheres completely overlap. In our particular case, $r_{\min}$ plays a role only for the BS interaction: due to the hard core repulsion, spheres of the same size are prevented from completely overlap, while a small sphere may happen to be totally included inside a big sphere.

Once the general expressions of the $\Omega_{\rm O}^{\alpha\beta}(r_{\alpha\beta})$ are known, it is important to bear in mind that the distance $r_{\alpha\beta}$ does not necessarily coincide with the distance between the two IPCs. Indeed, $r_{\alpha\beta} = r_{ij}$ only when $\alpha\beta$ = BB, while for $\alpha\beta$ = BS and = SS, $r_{\alpha\beta}$ is in general a function of r_{ij} and such a function depends on the relative orientation of the two IPCs. Consequently, the dependence of the total overlap volume is given by $\Omega_{\rm O_T}^{\alpha\beta} = \Omega_{\rm O_T}^{\alpha\beta}(r_{ij}, \theta_i, \theta_j, \theta_{ij})$.

We thus have an expression for the effective interaction between two IPCs, that can be evaluated in a fast and efficient way and that can readily be used in numerical approaches: for two interacting IPCs (separated by a distance and characterized by their orientation in space) the weight factors, $w_{\alpha\beta}$ are directly calculated via (at most) nine distances between the interaction spheres involved. The evaluation of the pair interaction between two IPCs does not require additional information.

4 Mapping between the DH and the CG model

As described in the previous section, our coarse grained model for IPCs is characterized by the following parameters: the interaction range between pair of particles, δ, the patch extension, γ, and the set of the three interaction strengths: $u_{\rm BB}$, between patch-free regions, $u_{\rm BS}$ between patch-free regions and patches, and $u_{\rm SS}$ between patches.

In the microscopic DH-model, the interaction range of the effective pair potential is determined by the screening conditions in the electrolytic solution. We assume δ of the coarse-grained interactions to be proportional to the Debye screening length according to the following relation: $\delta = n\kappa^{-1}$, with $n = 1, 2, 3, \cdots$; for simplicity we take integer n. Since in our approach we focus on rather large κ-values (high screening conditions), we only consider small n-values. The impact of different choices for n on the potential will be discussed in Sec. 5.

As mentioned above, in our coarse grained model, the patch extension γ is defined by the choice of e and ρ. We fix the eccentricity parameter of the coarse-grained model to have the same value of the asymmetry

parameter of the DH description, i.e., $e = a$. Thus, in our coarse-grained model, ρ depends only on δ, i.e., on the choice of n and on the screening conditions. Of course, the influence of the κ-value on the patch size has a physical background. Let us consider the possible realization of an IPC via the complexation of polyelectrolyte stars on the surface of an oppositely charged colloidal particle: a change in the salinity of the solution affects the degree of adsorption of the polyelctrolyte star[22] and, hence, its coverage of the colloidal surface (i.e., the extent of the patch).

We estimate the interaction strengths, u_{BB}, u_{BS}, and u_{SS}, by considering three characteristic reference configurations (index "rc") of two interacting IPCs, namely (see Fig. 5):

- the equatorial-equatorial (rc = EE) configuration: the two equators face each other and their mutual repulsion dominates the pair interaction;
- the equatorial-polar (rc = EP) configuration: a pole (patch) of one particle faces the equatorial region of the other particle, leading to a mutual attraction;
- the polar-polar configuration (rc = PP): a patch of one particle faces a patch of the other particle, leading to a repulsive interaction.

Evaluated from the analytic potential $\psi(r_{ij}, \theta_{i,\mathrm{rc}}, \theta^1_{i,\mathrm{rc}}, \theta^2_{i,\mathrm{rc}})$, the energy scale of each reference configuration is related to the three unknown parameters, u_{BB}, u_{BS} and u_{SS}. In the following we pursue two possible mapping schemes from the microscopic DH-model to the mesoscopic coarse-grained model:

1. We evaluate the overall strengths of the potential tails, obtained by integrating $\psi(r_{ij}, \theta_{i,\mathrm{rc}}, \theta^1_{i,\mathrm{rc}}, \theta^2_{i,\mathrm{rc}})$ over the range $2\sigma \leq r < \infty$, and we impose that they are equal to the corresponding expressions obtained by integrating $V(r, \theta_{i,\mathrm{rc}}, \theta_{j,\mathrm{rc}}, \theta_{ij,\mathrm{rc}})$ over the same range, i.e.,

$$u^{\mathrm{tot}}_{\mathrm{rc}} = \delta^{-1} \int_{2\sigma}^{\infty} \psi(r, \theta_{i,\mathrm{rc}}, \theta^1_{i,\mathrm{rc}}, \theta^2_{i,\mathrm{rc}}) dr \equiv \delta^{-1} \int_{2\sigma}^{\infty} V(r, \theta_{i,\mathrm{rc}}, \theta_{j,\mathrm{rc}}, \theta_{ij,\mathrm{rc}}) dr. \tag{19}$$

2. Alternatively, we relate the contact values of the two potential tails, i.e., we match

$$u^{\mathrm{max}}_{\mathrm{rc}} = \psi(2\sigma, \theta_{i,\mathrm{rc}}, \theta^1_{i,\mathrm{rc}}, \theta^2_{i,\mathrm{rc}}) \equiv V(2\sigma, \theta_{i,\mathrm{rc}}, \theta_{j,\mathrm{rc}}, \theta_{ij,\mathrm{rc}}). \tag{20}$$

The superscripts "tot" and "max" specify the two different types of mapping.

Since $V(r_{ij}, \theta_i, \theta_j, \theta_{ij})$ is different from zero only when $2\sigma \leq r_{ij} \leq 2\sigma + \delta$ and since, on such interparticle distances, the interaction energy is given by Eq. (13), we can explicitly write the mapping scheme as

$$\mathbf{u}^{\mathrm{m}}_{\mathrm{rc}} = \mathcal{M}^{\mathrm{rc}}_{\alpha\beta} \mathbf{u}^{\mathrm{m}}_{\alpha\beta}. \tag{21}$$

Here, "m" indicates one of the two the mapping schemes ("tot" or "max"). Further, $\mathbf{u}^{\mathrm{m}}_{\mathrm{rc}} = (u^{\mathrm{m}}_{\mathrm{EE}}, u^{\mathrm{m}}_{\mathrm{EP}}, u^{\mathrm{m}}_{\mathrm{PP}})$, $\mathbf{u}^{\mathrm{m}}_{\alpha\beta} = (u^{\mathrm{m}}_{\mathrm{BB}}, u^{\mathrm{m}}_{\mathrm{BS}}, u^{\mathrm{m}}_{\mathrm{SS}})$, and the coefficients of the 3×3 matrix, $\mathcal{M}^{\mathrm{rc}}_{\alpha\beta}$, depend on the geometric weights $w_{\alpha\beta}$ of the three reference configurations.

Once the parameters of the DH-model are fixed (Z_c, Z_s, ε, a and $\kappa\sigma$), the parameters of the coarse-grained model (δ, e and ρ) are chosen accordingly; choosing either mapping scheme introduced above, $\mathbf{u}^{\mathrm{m}}_{\mathrm{rc}}$ is evaluated and the $\mathbf{u}^{\mathrm{m}}_{\alpha\beta}$ are evaluated from inversion of Eqs. (21).

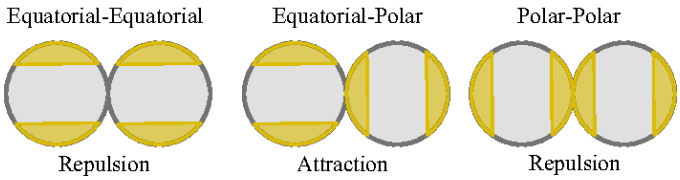

Figure 5: (Color online). Two dimensional representation of the three orientational configurations used as reference in the mapping between the analytic pair potential of Eqs. (7)-(8) and the coarse-grained model potential of Eq. (12). From left to right: equatorial-equatorial (EE), equatorial-polar (EP), and polar-polar (PP) configuration. The two IPCs are shown in contact, i.e., $r_{ij} = 2\sigma$.

5 Comparison between the DH and the CG model

Here, we consider the inverse patchy complexes described in Sec. 2 and we compare their microscopic pair interaction $\psi(r_{ji}, \theta_i, \theta_j, \theta_{ij})$ with the pair potential $V(r_{ij}, \theta_i, \theta_j, \theta_{ij})$ of the corresponding coarse-grained model described in Sec. 3 and 4. Concerning the microscopic system, we consider the dielectric medium to be water, in which case $\varepsilon = 80$ under normal conditions. We choose to deal with overall neutral particles and we set $Z_c = -180$ and $Z_p = 90$[9,16]. Besides being the simplest order case, this choice may be related to the fact that $|Z_c - 2Z_p|$ is small for IPCs with two patches, that result from the complexation of two polyelectrolyte stars onto an oppositely charged colloid[9]. Indeed, a big difference between the colloidal charge and the sum of charges of the two polyelectrolyte stars would lead to the adsorption of more than two polyelectrolyte stars onto the colloidal surface. We choose the asymmetry parameter of the charge distribution to be $a = 0.6\sigma$. The Debye screening length is a free parameter to be varied within the high screening range, i.e., $\kappa\sigma > 1$. As far as the coarse-grained model is concerned, we choose the interaction range to be determined by the Debye screening length, as described in Sec. 3. Since $e \equiv a$, then ρ is fixed once δ is chosen. The energy strengths of the three types of interaction are determined via both the above mentioned mappings, i.e., "tot" and "max". We compare $\psi(r_{ji}, \theta_i, \theta_j, \theta_{ij})$ and $V(r_{ij}, \theta_i, \theta_j, \theta_{ij})$, and we study how their agreement depends on the different mapping procedures (both for energies and interaction ranges) and on varying the screening conditions.

The Debye screening length sets the characteristic interaction range of the DLVO potential. Hence, we fix $\delta = 1/\kappa$ and we explore the screening range $2 < \kappa\sigma < 10$. We consider three characteristic configurations of the two IPCs at contact (namely, EE, EP and PP) and we translate/rotate one colloid with respect to the

other. The comparison between the analytic and the coarse-grained potential is shown in Fig. 6. The radial and the angular behaviors of the pair interaction are shown for both the energy mappings ("tot" and "max"): the procedure "max" allows a better quantitative agreement between our simple model and the DH description. Nonetheless, regardless of the chosen energy mapping, the main features and the symmetries of the analytic pair interaction are very well reproduced by the coarse-grained model, within the chosen screening range.

As explained in Sec. 3, we have the freedom of varying somewhat the parameter δ, by generalizing the relation $\delta = 1/\kappa$ into $\delta = n/\kappa$. The choice $n = 1$ is satisfactory for a wide range of screening conditions, but a closer agreement between the microscopic DH-system and the coarse-grained model may be achieved by tuning n. By fixing the screening length to an intermediate value within the previously studied screening range, i.e., $\kappa\sigma = 5$, we focus on the effect of the interaction range. We set $n = 1, 2,$ and 3 and we consistently choose ρ. Fig. 7 and Fig. 8 show the radial and the angular dependence of the interaction energy between a pair of IPCs. We observe that the choice $n = 3$ brings a better agreement between the microscopic potential and the coarse-grained one in both energy mapping procedures. As we learn from the case $\kappa\sigma = 5$, the interaction range, and consequently the patch extension, can be tuned with respect to the screening conditions: larger n values guarantee a more quantitative agreement for larger $\kappa\sigma$. Specifically, when $\kappa\sigma$ ranges from 2 to 10, then n spans monotonically the range between 1 and 4. The corresponding change of ρ with n is found to show a trend towards smaller patches as $\kappa\sigma$ increases. When considering IPCs as coming out of the adsorption of polyelectrolyte stars onto oppositely charged colloids, the correlation between the patch size and the screening conditions may be related to different degrees of adsorption. Indeed, on adding salt (i.e., increasing $\kappa\sigma$) the adsorbed polyelectrolyte stars change conformation[9] and, hence, their surface coverage onto the colloid shrinks.

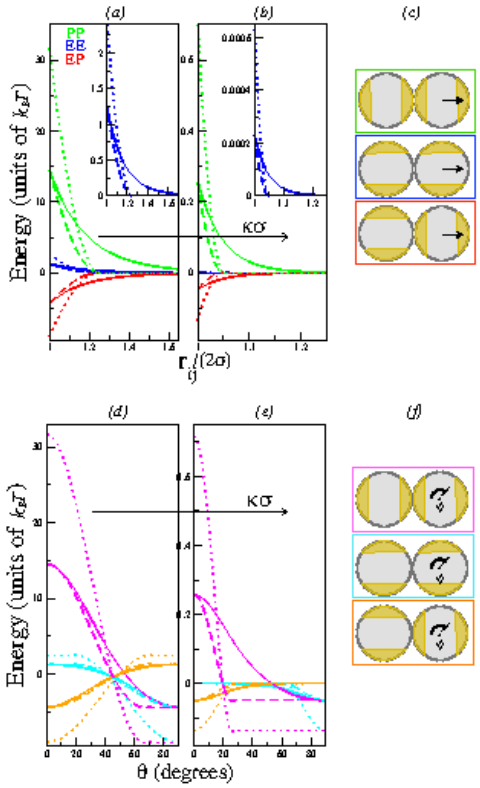

Figure 6: (Color online). Three top panels: interaction energy between two IPCs as a function of their distance r_{ij} for three fixed orientations of the two IPCs: PP (green), EE (blue), and EP (red), as shown schematically in panel (c) for particles at contact. Three bottom panels: interaction energy between the two IPCs at distance $r_{ij} = 2\sigma$ as a function of the rotation angle θ around a chosen axes. We consider two IPCs in a reference configuration, namely PP (magenta), EE (cyan), and EP (orange), and we rotate one of the two IPCs around the axes $\hat{v}$, as shown in panel (f). Two different screening conditions are chosen: $\kappa\sigma = 2$ in panels (a) and (d), and $\kappa\sigma = 10$ in panels (b) and (e). Continuous lines correspond to the analytic pair potential of Eqs. (7) and (8), where the microscopic parameters are $Z_c = -180$, $Z_p = 90$, $\varepsilon = 80$, and $a = 0.6\sigma$. Dotted lines correspond to the coarse-grained potential of the mapping procedure "tot" for the energy strengths, and dashed lines correspond to the procedure "max" (see text). For both types of energy mapping, the interaction range of the coarse-grained model is fixed to $\delta = 1/\kappa$ on changing the screening lengths.

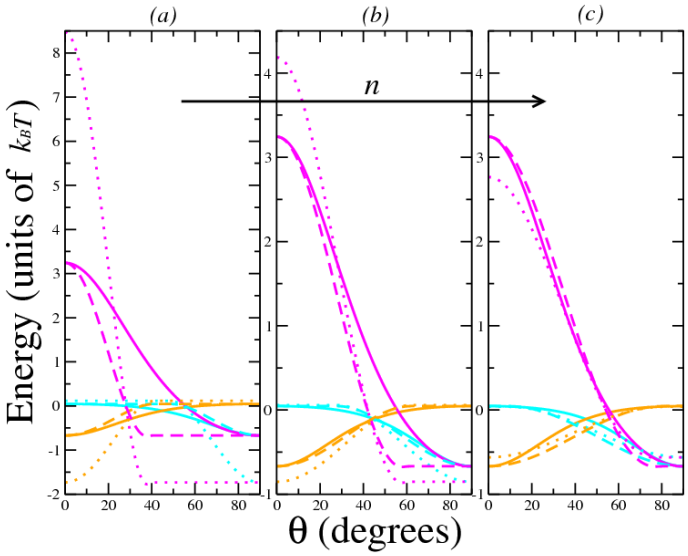

Figure 7: (Color online). Interaction energy between two IPCs as a function of their distance r_{ij}. Three fixed orientations of the two IPCs are chosen: PP (green), EE (blue), and EP (red), as shown schematically in panel (c) of Fig. 6. Continuous lines correspond to the analytic pair potential of Eqs. (7) and (8), where the microscopic parameters are $Z_c = -180$, $Z_p = 90$, $\varepsilon = 80$, $a = 0.6\sigma$ and $\kappa\sigma = 5$. Dotted lines correspond to the coarse-grained potential of the mapping procedure "tot" for the energy strengths, and dashed lines correspond to the procedure "max" (see text). For both mappings, the choice of the interaction range is determined by the Debye screening length, i.e., $\delta = n/\kappa$. From left to right: $n = 1, 2,$ and 3, i.e. $\delta = 0.2\sigma$ in panel (a), $\delta = 0.4\sigma$ in panel (b), and $\delta = 0.6\sigma$ in panel (c). The insets in the three panels show an enlargement around small energy values, in order to better visualize the EE pair interaction.

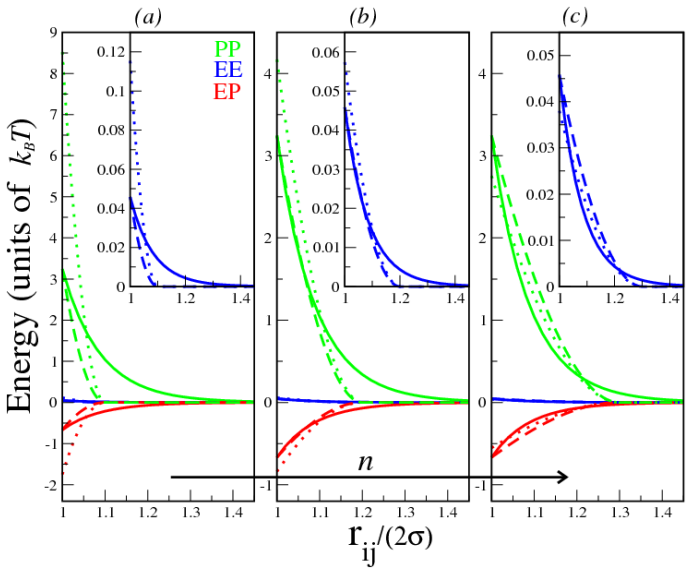

Figure 8: (Color online). Interaction energy between two IPCs at a fixed distance $r_{ij} = 2\sigma$ as a function of the rotation angle θ around a chosen axes. We consider two IPCs in a reference configuration, namely EE (cyan), EP (orange), and PP (magenta), and we rotate one of the two IPCs around the axes $\hat{v}$, as shown in panel (f) of Fig. 6. Continuous lines correspond to the analytic pair potential of Eqs. (7) and (8), dotted lines correspond to the coarse-grained potential of the mapping procedure "tot", and dashed lines correspond to mapping procedure "max" (see text). All the parameters are the same as in Fig. 7, hence in panel (a) $\rho = 0.5\sigma$ and $\gamma \approx \pi/8$, in panel (b) $\rho = 0.6\sigma$ and $\gamma \approx \pi/6$, and in panel (c) $\rho = 0.7\sigma$ and $\gamma \approx \pi/4$.

6 Conclusions

In the present paper, we consider negatively charged colloids with two positively charged regions located on opposite poles. Such heterogeneously charged colloids can be viewed as spherical particles with patterned surfaces: a patch-free equatorial region and two extended polar patches (see Fig. 1). For two interacting IPCs, the equatorial regions and the poles are mutually repulsive while the patch and equatorial regions attract each other. We refer to this class of systems as inverse patchy colloids in order to stress the mutual repulsive nature of the charged-like patches, in contrast to attractive patches on typical patchy colloids.

Based on the Debye-Hückel approach, we derive an analytical description of the pair interaction between two IPCs with two polar patches. In parallel, we propose a coarse-grained patchy model which reproduces the symmetries of the charge pattern on the colloidal surface. Taking advantage of a mapping procedure from the microscopic DH description, we establish a well defined connection between the mesoscopic coarse grained model and the IPC model system we refer to.

A possible realization of the studied IPCs is provided by a new variety of complex particles coming out of the absorption of soft polyelectrolyte stars on the surface of oppositely charged colloids[9]. It has been shown that the equilibrium features and self-assembly of such systems can be externally tuned; for instance, the extent and strength of the patch can be controlled either by using different stars or by changing the salinity of the solution, resulting in a number of distinct adsorption configurations[22]. The present model is most suited for tight adsorption of the polyelectrolyte stars onto the colloids and becomes increasingly

more approximate for systems in which the salt concentration or the charge ratio of the two components are such that the detachment of the polyelectrolytes from the colloidal surface is significant. An indispensable prerequisite of the applicability of our model is that the center of charge of the polyelectrolyte stars do not lie outside the surface of the colloid, so that the majority of chains are expected to be attached on the surface. In such cases our model maintains the salient features of the microscopic system. It is possible to argue that, by varying the ratio between the colloid- and polyelectrolyte stars- charges and the relative sizes of the two components, more than two polyelectrolytes stars will adsorb onto the colloidal surface. The resulting complex will have a number bigger than two of positive patches attached onto the negative colloidal surface. In these cases, the advantage of the coarse-graining procedure is of great importance and provides great advantages in comparison with the microscopic model. Fig. 9 illustrates the situation: whereas in the microscopic description for a case of, e.g., three adsorbed polyelectrolyte stars, we would end up with a complicated interaction involving series of spherical harmonics, the coarse-grained model allows us to place patches at selected points and proceed with, e.g., a simulation of the system in which only the calculation of overlapping volumes is needed: the latter task is computationally straightforward. In this sense, our model bears the simplicity of previously developed Kern-Frenkel types of models but at the same time it retains the salient quantitative characteristics of the underlying microscopic details in a quantitative manner.

We introduced inverse patchy colloids as a novel class of patchy particles, using the general mechanism of *charge heterogeneity*[18,23–25] as a means of producing the effect of repulsive patches, which at the same time are attracted to the parts of the colloidal surface that are not covered by the patch. Evidently, the same goal can also be achieved by appropriate chemical treatment of the respective colloidal surfaces. The salient physical property of IPC's is a combination between anisotropy and competing interactions, which are expected to bring about quite unusual kinds of new phenomena. For instance, even the simplest form of IPCs, the two-patch polar/equatorial model, frustration between the various, anisotropic contributions emerges, which is expected to lead to the formation of nontrivial ordered structures. In the case of standard patchy colloids, the varieties of crystalline structures that emerge have started to be investigated and they include a number of ordered configurations[26–28], including the recently discovered stability region of the Kagome lattice[29,30]. Inverse patchy colloids offer a new paradigm to be investigated, in which both the competition between attractions and steric constraints and the transition from two to three dimensions are factors of crucial importance. Order can also be *local*, in the sense that templated self-assembly of well-defined, small clusters can be driven[31,32] or that larger, more amorphous clusters can grow[33,34]. It remains to be seen which of these scenarios materialize for IPCs and under which conditions of patchiness, energy and length scales involved.

A complementary set of questions pertains also to the disordered phases of IPCs, for which phase separation for patchy systems[35–39] and its dependence on the patch characteristics has occupied the literature on standard patchy colloids quite extensively. Associated with it is the existence of possible glassy or gel phases, which has been amply investigated for patchy colloids[40–43] but not for IPCs; see, however, very recent work on the somewhat similar system of Laponite[44], in which T-like configurations of the particles are preferred.

The next question to be addressed, therefore, is *how do inverse patchy colloiss differ from standard patchy colloids in their macroscopic behavior?* In this context, it is worth noting that a correspondence between the patch number/geometrical arrangement and the bonding pattern is an important feature determining the properties and the structure of systems with attractive patches. Such a feature is no longer

present when considering patchiness as emerging from heterogeneously charged particles. The main feature of such patchy systems is not anymore the limited valence in bonding, but rather a competitive interplay between attractive and repulsive anisotropic interactions. We believe that the class of inverse patchy colloids introduced here constitutes a broad new open field, and the work at hand could offer a foundation for its further development.

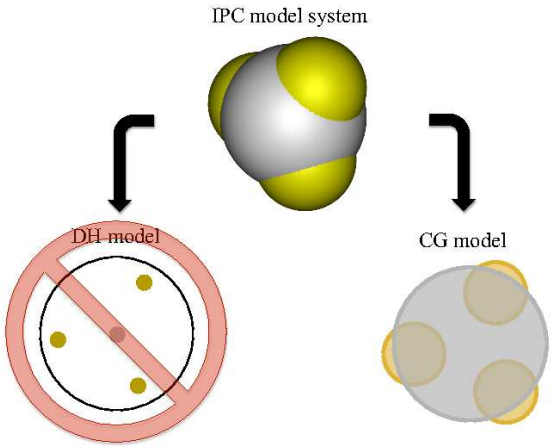

Figure 9: (Color online). Top: three-dimensional representation of an inverse patchy colloidal particle with three patches arranged on an equilateral triangle lying on the equatorial plane. The (yellow) patches and the (grey) patch-free region have different surface charges. Bottom: the Debye-Hückel scheme (left side) and the mesoscopic coarse-grained model (right side). The DH model is shown as "forbidden": even though possible in principle, the analytical treatment for the effective pair interaction is of prohibitive complexity. The connection from the microscopic to the mesoscopic model is thus not shown because the mapping might be hardly feasible. On the other hand, the coarse-grained model of an IPC with three patches is still available, once a reasonable choice of the parameters is made.

Acknowledgments

The authors thank Ronald Blaak for valuable comments. EB wishes to thank the Alexander von Humboldt Foundation for financial support through a Research Fellowship as well as the Austrian Research Fund (FWF) for support through a Lise-Meitner Fellowship under project number M 1170-N16. Additional support by the DFG is acknowledged.

A The Debye-Hückel approximation

In this Appendix, we investigate the ranges of the model parameters for which the Debye-Hückel approximation is appropriate. To this end we start from the *non-linear* Poisson-Boltzmann differential equation[11]

describing the electrostatic potentials in the ionic solution, valid for $r > \sigma$:

$$\nabla^2\Phi^{\mathrm{II}}(r,\theta) = -\frac{4\pi}{\varepsilon}\sum_i Z_i q_e \rho_i^0 \exp\left(-\frac{Z_i q_e \Phi^{\mathrm{II}}(r,\theta)}{k_B T}\right), \tag{22}$$

where the parameters have been specified in Sec. 2.1. In the Debye-Hückel approximation, the right-hand-side of above equation is linearized under the assumption of low ion concentrations. Indeed, expanding the exponential and truncating it at the first order, one obtains

$$\exp\left(-\frac{Z_i q_e \Phi^{\mathrm{II}}(r,\theta)}{k_B T}\right) \approx 1 - \frac{Z_i q_e \Phi^{\mathrm{II}}(r,\theta)}{k_B T}. \tag{23}$$

Summing over the index i and taking into account electroneutrality of the solution, the right hand side of the Poisson-Bolzmann equation becomes $\kappa^2\Phi^{\mathrm{II}}(r,\theta)$, where κ has been defined in Sec. 2.1. The Debye-Hückel approximation is meaningful only if $q_e\Phi^{\mathrm{II}}(r,\theta) \lesssim k_B T$; this implies that, assuming ambient conditions, $q_e\Phi^{\mathrm{II}}(\sigma,\theta)$ has to be at least smaller than 26 meV.

Let us define $x = q_e\Phi(r,\theta)/k_B T$, where $\Phi(r,\theta)$ is given by Eq. (2). We set $Z_c = -180$, $Z_p = 90$ (neutral particles), and $\varepsilon = 80$ (dielectric permittivity of water under normal conditions). By considering different a parameters and screening conditions, we determine the range of particle sizes for which $x \lesssim 1$. We estimate the size of the particle for which the Debye-Hückel approximation is valid to range from a few tens of nanometers to some microns, on changing the asymmetry parameters between 0.2σ and 0.8σ, in different screening conditions ($1 < \kappa\sigma < 100$).

We note that for colloidal sizes and charges σ and Z_c fulfilling the condition

$$\sigma/\mathrm{nm} \gtrsim 0.1\, Z_c \tag{24}$$

no charge renormalization is needed[45,46].

B Treatment of the analytic electrostatic potential

In this Appendix, we explicitly show that, in high screening conditions, a Yukawa-like expression represents a good approximation for the total electrostatic potential given in Eq. (2). In particular we focus on the ratio between Bessel functions of consecutive orders, occurring in Eq. (2), i.e.

$$R_l(\kappa r) \equiv \frac{1}{\kappa\sigma\sqrt{r\sigma}}\frac{K_{l+1/2}(\kappa r)}{K_{l+3/2}(\kappa\sigma)}. \tag{25}$$

The first three modified spherical Bessel functions of the third kind (i.e., $l = 0,1,2$) read[19]

$$\begin{aligned} K_{1/2}(z) &= \sqrt{\frac{\pi}{2}}\frac{\exp(-z)}{\sqrt{z}} \\ K_{3/2}(z) &= \sqrt{\frac{\pi}{2}}\frac{\exp(-z)}{\sqrt{z}}(1+z^{-1}) \\ K_{5/2}(z) &= \sqrt{\frac{\pi}{2}}\frac{\exp(-z)}{\sqrt{z}}(1+3z^{-1}+3z^{-2}). \end{aligned} \tag{26}$$

For $l = 0$

$$R_0(\kappa r) = \frac{\exp(\kappa\sigma)}{1+\kappa\sigma}\frac{\exp(-\kappa r)}{r}, \tag{27}$$

while for $l = 1$

$$R_1(\kappa r) = \frac{\exp(\kappa\sigma)}{1+\kappa\sigma}\frac{\exp(-\kappa r)}{r}\frac{\kappa r+1}{\kappa r}\frac{(\kappa\sigma)^2+\kappa\sigma}{(\kappa\sigma)^2+3\kappa\sigma+3}. \tag{28}$$

For high screening conditions $(\kappa\sigma \gg 1)$, $R_1(\kappa r)$ simplifies and reduces to $R_0(\kappa r)$, i.e.

$$R_1(\kappa r) \simeq \frac{\exp(\kappa\sigma)}{1+\kappa\sigma}\frac{\exp(-\kappa r)}{r} = R_0(\kappa r). \tag{29}$$

The general structure of the algebraic expressions in Eq. (26) leads to the conclusion that $R_i(\kappa r) \approx R_0(\kappa r)$ for $i \geq 2$. Therefore, under assuming high screening conditions, the analytic potential $\Phi(r,\theta)$, given in Eq. (2), can be written in the Yukawa-like form, given in Eqs. (3) and (4).

In Fig. 10 we present numerical results for the comparison between the analytic electrostatic potential and the Yukawa-like, simplified form. In the explored parameter range, the approximate expression for the electrostatic potential is found to be reasonably close to the analytic potential, even right at the particle surface.

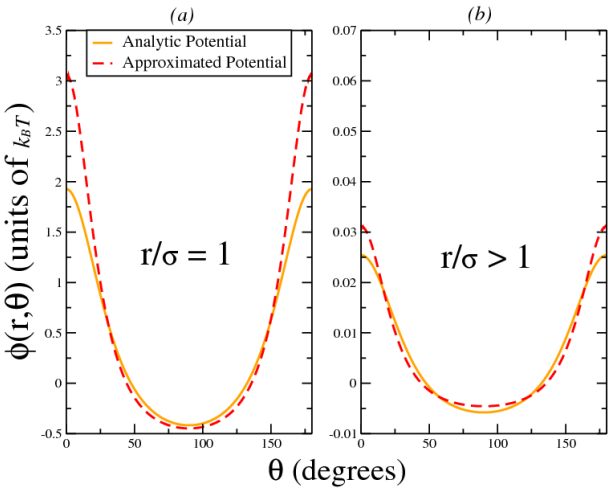

Figure 10: (Color online). Comparison between the analytic electrostatic potential of Eq. (2) and the Yukawa-like simplified potential of Eqs. (3) and (4) for the following set of parameters: $Z_c = -180$ and $Z_p = 90$, $a = 0.6\sigma$ and $\kappa\sigma = 5$. Panel (a): comparison of the surface potential $\Phi(\sigma,\theta)$ as a function of θ. Panel (b): comparison between the two potential forms as a function of θ at a distance $r/\sigma = 1+4/(\kappa\sigma)$ from the field source.

References

[1] A. B. Pawar and I. Kretzschmar, *Macromol. Rapid. Commun.*, 2010, **31**, 150.

[2] E. Bianchi, R. Blaak and C. N. Likos, *Phys. Chem. Chem. Phys.*, 2011, **13**, 6397.

[3] G. Zhang, D. Wang and H. Möhwald, *Chem. Mater.*, 2006, **18**, 3985.

[4] A. B. Pawar and I. Kretzschmar, *Langmuir*, 2009, **25**, 9057.

[5] A. M. Yake, C. E. Snyder and D. Velegol, *Langmuir*, 2007, **23**, 9069.

[6] D. J. Kraft, J. Groenewold and W. K. Kegel, *Soft Matter*, 2009, **5**, 3823.

[7] Y. S. Cho, G. R. Yi, S. H. Kim, M. T. Elsesser, D. R. Breed and S. M. Yang, *J. Colloid Interface Sci.*, 2008, **318**, 124.

[8] V. Rastogi, A. A. Garca, M. Marquez and O. D. Velev, *Macromol. Rapid Commun.*, 2010, **31**, 190.

[9] C. N. Likos, R. Blaak, and A. Wynveen, *J. Phys.: Condens. Matter*, 2008, **20**, 494221.

[10] J. D. Jackson, *Classical Electrodynamics*, Wiley, New York, 3rd edn., 1999.

[11] W. B. Russel, D. A. Saville and W. R. Schowalter, *Colloidal Dispersions*, Cambridge University Press, Cambridge, 1989.

[12] P. Debye and E. Hückel, *Physikalische Zeitschrift*, 1923, **24**, 185.

[13] C. N. Likos, *Phys. Rep.*, 2001, **348**, 267.

[14] M. J. Stevens, M. L. Falk and M. O. Robbins, *J. Chem. Phys.*, 1996, **104**, 5209.

[15] A. R. Denton, *J. Phys.: Condens. Matt.*, 1999, **11**, 10061.

[16] D. El Masri, P. van Oostrum, F. Smallenburg, T. Vissers, A. Imhof, M. Dijkstra and A. van Blaaderen, *Soft Matter*, 2011, **7**, 3462.

[17] E. J. W. Verwey and J. T. G. Overbeek, *Theory of the stability of lyophobic colloids*, Elsevier, Amsterdam, 1948.

[18] N. Hoffmann, C. N. Likos, and J.-P. Hansen, *Mol. Phys.*, 2004, **102**, 857.

[19] M. Abramowitz and I. A. Stegun, *Handbook of Mathematical Functions: with Formulas, Graphs, and Mathematical Tables*, Dover Publications, 1965.

[20] Implicit here is the change of variables from $(\theta_i, \theta_j, \theta_{ij})$ to $(\theta_i, \theta_i^1, \theta_i^2)$. Though this does change the functional form of the function ψ_{ij}, we employ thereafter the same symbol for reasons of parsimony in notation.

[21] N. Kern and D. Frenkel, *J. Chem. Phys.*, 2003, **118**, 9882.

[22] M. Konieczny and C. N. Likos, *Soft Matter*, 2007, **3**, 1130–1134.

[23] C. N. Likos, R. Blaak and A. Wynveen, *J. Phys: Condens. Matter*, 2008, **20**, 494221.

[24] E. Eggen and R. van Roij, *Phys. Rev. E*, 2009, **80**, 041402.

[25] N. Boon, E. C. Gallardo, S. Zheng, E. Eggen, M. Dijkstra and R. van Roij, *J. Phys.: Condens. Matter*, 2010, **22**, 104104.

[26] E. G. Noya, C. Vega, J. P. K. Doye and A. A. Louis, *J. Chem. Phys.*, 2010, **132**, 234511.

[27] F. Romano, E. Sanz and F. Sciortino, *J. Chem. Phys.*, 2010, **132**, 184501.

[28] G. Doppelbauer, E. Bianchi and G. Kahl, *J. Phys.: Condens. Matter*, 2010, **22**, 104105.

[29] Q. Chen, S. C. Bae and S. Granick, *Nature*, 2011, **469**, 381.

[30] F. Romano and F. Sciortino, *Nat. Mater.*, 2011, **10**, 171.

[31] A. J. Williamson, A. W. Wilber, J. P. K. Doye and A. A. Louis, *Soft Matter*, 2011, **7**, 3423.

[32] A. W. Wilber, J. P. K. Doye and A. A. Louis, *J. Chem. Phys.*, 2009, **131**, 175101.

[33] L. Hong, A. Cacciuto, E. Luijten and S. Granick, *Langmuir*, 2008, **24**, 621.

[34] F. Sciortino, A. Giacometti and G. Pastore, *Phys. Rev. Lett.*, 2009, **103**, 237801.

[35] J. Russo, J. M. Tavares, P. I. C. Teixeira, M. M. Telo da Gama and F. Sciortino, *Phys. Rev. Lett.*, 2011, **106**, 085703.

[36] A. Reinhardt, A. J. Williamson, J. P. K. Doye, J. Carrete, L. M. Varela and A. A. Louis, *J. Chem. Phys.*, 2011, **134**, 104905.

[37] E. Bianchi, P. Tartaglia, E. Zaccarelli and F. Sciortino, *J. Chem. Phys.*, 2008, **128**, 144504.

[38] G. Foffi and F. Sciortino, *J. Phys. Chem. B*, 2007, **111**, 9702.

[39] C. W. Hsu, J. Largo, F. Sciortino and F. W. Starr, *Proc. Nat. Acad. Sci. U.S.A.*, 2008, **105**, 13711.

[40] E. Bianchi, P. Tartaglia, E. La Nave and F. Sciortino, *J. Phys. Chem. B*, 2007, **111**, 11765.

[41] S. Corezzi, C. De Michele, E. Zaccarelli, D. Fioretto and F. Sciortino, *Soft Matter*, 2008, **4**, 1173.

[42] J. Russo, P. Tartaglia and F. Sciortino, *J. Chem. Phys.*, 2009, **131**, 014504.

[43] J. M. Tavares, P. I. C. Teixeira, M. M. Telo da Gama and F. Sciortino, *J. Chem. Phys.*, 2010, **132**, 234502.

[44] B. Ruzicka, E. Zaccarelli, L. Zulian, R. Angelini, M. Sztucki, A. Moussaïd, T. Narayananand and F. Sciortino, *Nat. Mater.*, 2011, **10**, 56.

[45] S. Alexander, P. M. Chaikin, G. J. M. P. Grant and P. Pincus, *J. Chem. Phys.*, 1984, **80**, 5776.

[46] M. O. Robbins, K. Kremer and G. S. Grest, *J. Chem. Phys.*, 1988, **88**, 3286.

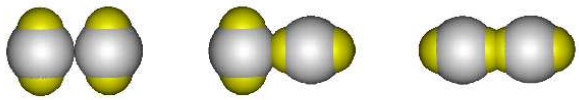

Figure 11: (Color online) **Table of contents Figure**. Charged colloids with adsorbed patches of opposite charge form a new class of inverse patch colloidal particles, which are analyzed and coarse-grained in this paper.